

Operational Station Horizontal Plane Motion Maneuvering of FPSO in Shallow and Deep Water

¹Orji, U. Charles, ²Dokubo, K. Daniel, ³Ibitoru F. Dick

^{1,2,3}(Center of Excellence in Marine and Offshore Engineering, Rivers State University, P.M.B. 5080, Port Harcourt, Rivers State, Nigeria)

Corresponding Author: Dokubo, Daniel Koriota-a

ABSTRACT: Floating Production and offloading (FPSO) systems have become the leading offshore structure deployed in the oil and gas industry. Their station keeping capacity is usually possible with the use of mooring lines which are anchored to the sea bed. The challenge however is that the response of an FPSO in shallow and deep water have very different results. Studies have shown that the deep-water environment can easily be modeled as the challenges in deep-water are easily known and can be managed, however this is not the case in shallow water. Thus, this thesis aims to explain and show the reasons behind the possible differences in the motion response behavior of an FPSO in shallow and deep-water scenarios in 3 degrees of freedom (surge, sway and yaw). An analytical solution is achieved considering the Froud Krylov and diffraction forces in the surge, sway and yaw directions, a time series relationship is obtained statistically. The analysis was done for wave elevations of 6m 4m and 2m respectively at frequencies of 0.3,0.4,0.5 and 0.6 rad/s. The developed procedure which is coded in MATLAB was validated against ORCAFLEX simulation for a deep-water wave condition of surface elevation of 6m and frequency of 0.6rad/s for a similar vessel. The result for a 30s simulation showed an error margin of between 4.1%, 12.1% and 15.6 % for the surge, sway and yaw motions respectively. The results from the estimated motions for the different scenario showed the influence of water depth on the response of an FPSO such that in shallow water there tends to be more motion due to the velocity of the water which has significant effect as the distance from the seabed to the hull is short and as such the velocity does not wear out and the low effect of damping from the mooring lines, whereas in deep water the response is smaller as the damping effect from the mooring lines have significant effect on the FPSO's response. There also was seen a significant percentage difference between the shallow and deep-water hydrodynamic forces in the surge and sway direction in a number of cases the shallow water force was more than 50% different from the surge force which shows the reason why the motion in shallow water is more than that of the deep water.

KEYWORDS FPSO, shallow water, deep water, analysis, maneuvering.

Date of Submission: 26-05-2021

Date of acceptance: 09-06-2021

I. INTRODUCTION

Total oil production in the year 2000 from offshore locations accounted for about 22% of global production and 1% of this came from deep water. As of 2010 these figures had soared to about 33% and 7% respectively and by 2015 the latter is expected to bounce up to 11% [1]. Furthermore, the average depth of installing subsea wells has seen a tremendous increase from about 200m in early 90s to about 1000m as of 2013 [2] and even beyond 1000m as of today. As such the offshore industry has continuously reached to new frontiers since its inception as can be seen from the figure below.

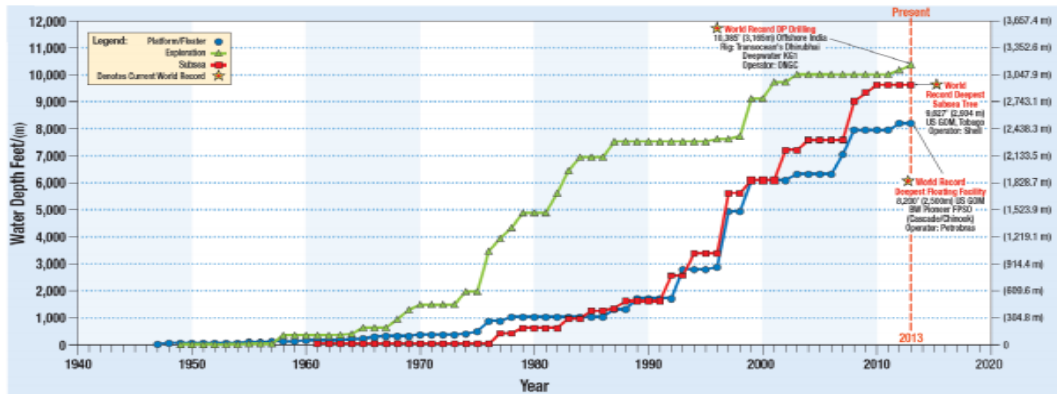


Figure 1 – Trend in water Depth for offshore Production [3]

Interestingly, it would seem more likely that operations in the shallow water should be less challenging than that of deep water but unfortunately there have been some unanswered questions as to why the reverse is the case. It would seem logical that the deeper you go into the ocean from deep to ultra-deep the challenges should be worsened, however in most cases the challenges of the deep-water environment can already be predicted and planned for, but in the case of shallow water the effects have proven challenging.

As some of the challenges may not be fully understood, this project aims to compare and analyze the maneuvering capacity of an FPSO in both shallow water and deep water by typically looking at the loading effect on a structure (typically a moored FPSO) subjected to the hydrodynamic environment in deep water and in shallow water to better explain some of the unknowns.

This project would enable to be more informed of the challenges that exists in both shallow and deep-water scenarios, and in the event that certain details are yet unknown a much better safety factor can be inputted in the design phase to cater for the cases of uncertainty.

Different standards have different ranges to define water depths for deep and shallow waters, but for the purpose of this thesis deep water would be defined with water depths above 300m and shallow water would be defined as water depth below 300m by industry practice.

It is important to note that a FPSO cannot produce oil and gas in isolation, it definitely would require other offshore production systems such as the sub-sea production systems (SPS), umbilicals, flow lines and risers (UFR), mooring lines, shuttle tankers, offloading buoy e.t.c. as shown in figure 2 below.



Figure 2 - Offshore production systems

Hydrodynamic and structural analysis take predominant roles in hull design on the grounds of safety, environment and economy. This unit is designed to be on site for a specific number of years usually 25 years without dry docking and as such should be built to withstand environmental loads in such a way that the structure does not go outside of a predetermined envelop, which means its sea keeping feature and its station maneuvering is and should remain a top priority.

II. MATERIAL

The FPSO is such that it gets its payload support from its buoyancy, the environmental loads are resisted by vessel inertia and stability as well as mooring strength [4].

To accurately predict the response of a turret moored FPSO is often a daunting task. There are quite a number of coupling terms and the FPSO's global performance tends to be sensitive to variations in design parameters. Although model testing has the limitations of Reynolds number discrepancies, physical dimensions and current turbulence etc, when combined with numerical approach can be very effective in validating results

[5]. The response in shallow water and deep water are not expected to be the same, in very shallow water depths it is important that the motion performance of the FPSO is researched thoroughly for production and safety due to the fact that the vessel may be damaged due to touching the sea bed in such shallow conditions [6]. In deep waters, the responses of mooring lines become more significant and difficult to be accurately captured using experimental approach [7].

Although this research is geared towards an understanding of the motion response of an FPSO it would be of great importance to see what happens to other vessel types. According [8] a balance between the inertial forces, moments and hydrodynamic actions on the ship's hull, propeller(s), and rudder(s) is essential to the dynamic equilibrium of a moving vessel. More so, it would be essential to understand this balance between the inertia, moments and hydrodynamic action on an FPSO as it plays a major role in the station maneuvering of the vessel. In shallow water, the limited water depth will change the pressure distribution around the vessel and lead to increase in hydrodynamic forces [9]. It is important to note that the maneuvering forces on a vessel are most commonly evaluated using a ship-based axis system [10].

FPSO's are usually fitted with mooring lines, these are used mainly for station keeping of the floating unit and is made up of anchors, mooring lines, fairleads, tuggers and winches. There are several types of mooring system used offshore based on the type of mooring line and its configuration. Majority of the mooring systems are: steel chain catenary, wire catenary and taut polyester line, the main mooring line configurations used in the offshore industry are turret moored systems or spread moored systems. Anchors provide the holding power to the FPSO either by burying it into the seabed or by sheer mass or a combination of both.

In offshore locations where FPSO's are used, the FPSO's are stationed mostly through the use of a mooring system which could either be spread moored or turret moored. The primary criteria for the choice of the type of mooring system to be used is the prevailing environmental conditions in the region. For example, most of the FPSO's in West of Africa (WoA) are spread moored as the conditions in this region is relatively calm (H_s of about 5m and T_p of 17s) although in some areas there are turret moored FPSO's and a typical example is the Shell SEAEAGLE situated in southern part of Nigeria. The mooring system provides the restoring force for the floating unit and can have significant effect on the motion response in deep water. The effect of mooring lines in shallow waters due to environmental loads are relatively small, however at greater depths the mooring lines significantly affect the behavior of the system. Research has shown that the damping from the mooring lines affect significantly the low frequency motions and mooring line tensions of an FPSO [11].

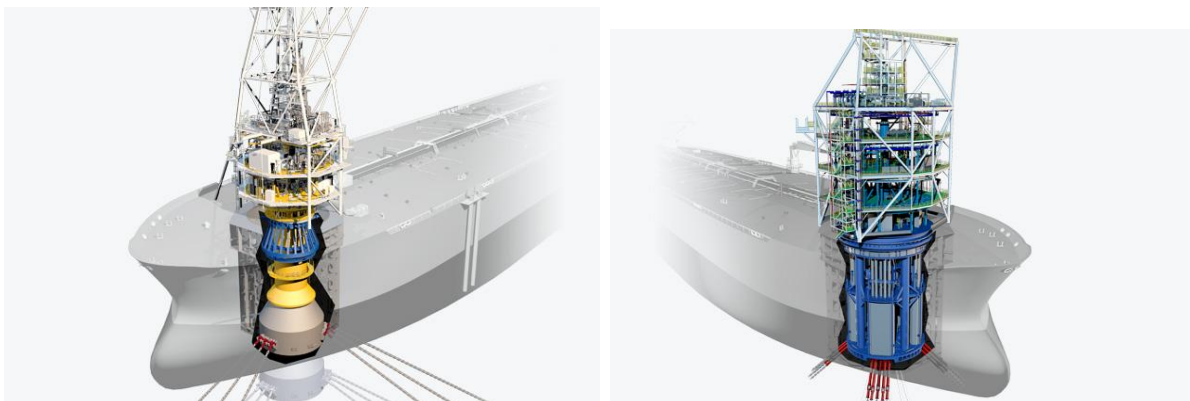


Figure 2.4 – Internal disconnectable and Internal permanent turret mooring system for FPSO

Design Loads: The structural design of the hull of an FPSO needs proper and adequate considerations for both still water loads, environmental loads and accidental loads. The still water loads vary between the ballast and full load conditions and the still water conditions are defined in the FPSO's manual however the environmental loads are described through the statistical metocean data. The focus of this thesis would be based on environmental loads.

In general, there exists Functional Loads (These refer to loads that arise due to physical existence of the riser during operational and installation processes but neglecting environmental or accidental effects [12]), environmental loads (these are induced by waves, wind and current) and accidental loads (these refer loads and motions that are caused by accidental occurrences).

From a global analysis perspective, shallow water FPSO system can be much more challenging to analyze and design than ultra-deep-water systems this is due to the environmental loading on the system in shallow water, the hardening nonlinear stiffness of the mooring system that at extreme offsets could result in

large variable loads, a low level of associated damping in the system and design an appropriate riser system fluid transfer [13].

The metocean parameters which define the environment are of primary importance as these metocean parameters include local surface wind, swells, current, tidal flows and waves [14].

III. METHODOLOGY

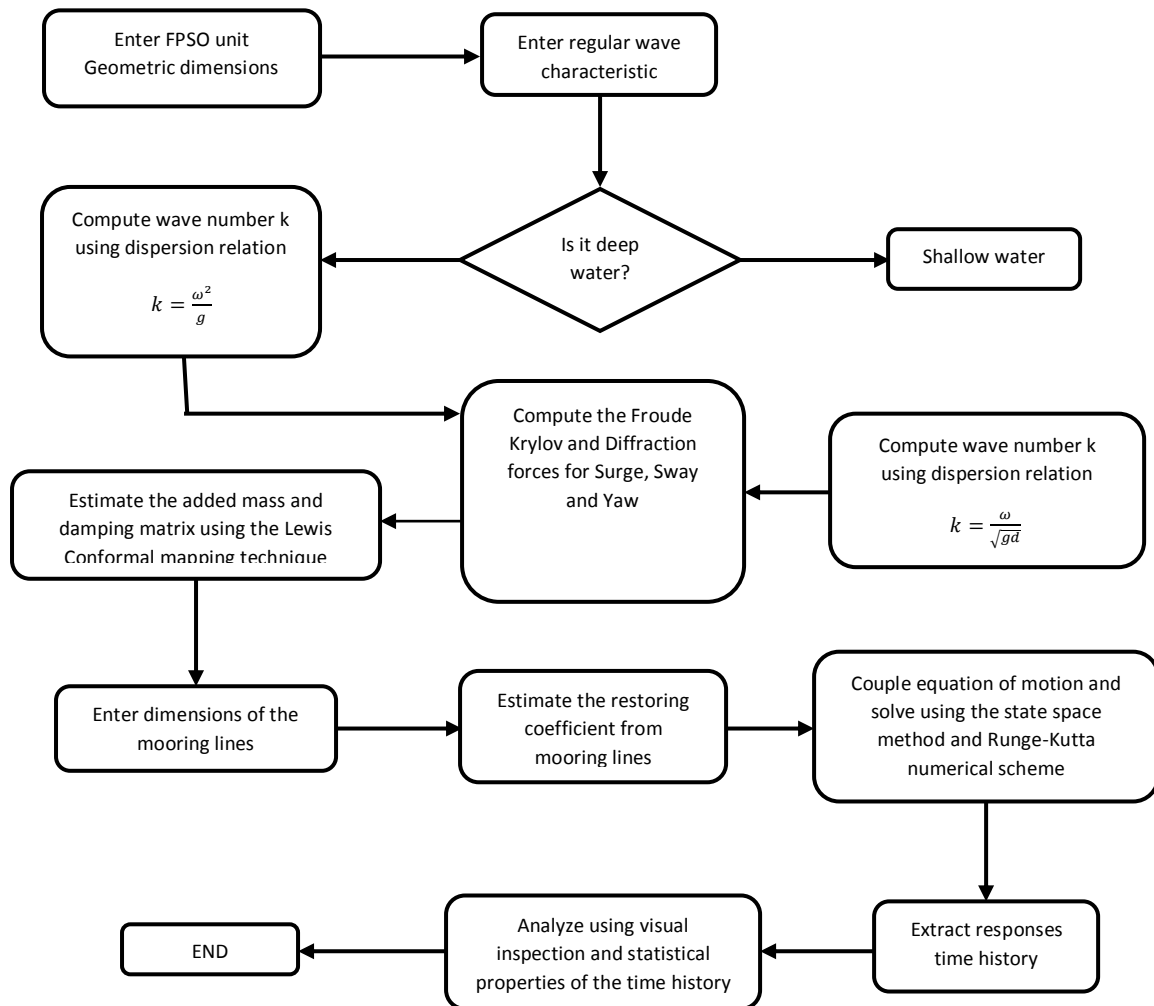


Figure 4 (a) Analysis Flow Path

The FPSO is simply modelled as a rectangular cylinder, assumed to be slender, the unit is shown moored according to figure 4

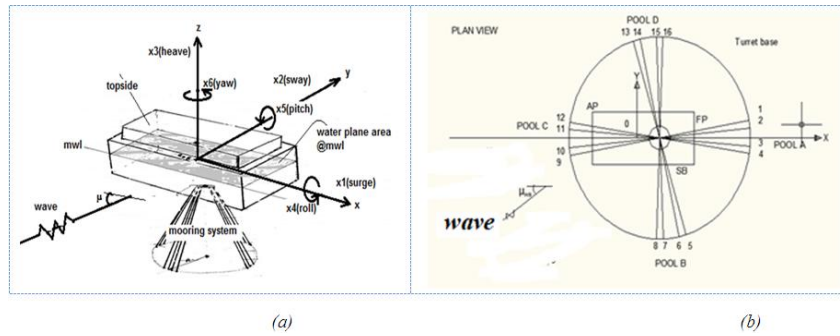


Figure 5 (a) Schematic diagram of model moored FPSO (b) Plan View of FPSO model;

Equation of motion

The equation of motion resulting from the balancing of forces acting on floating unit using the popular Newton’s law of motion is used to model the dynamic system of the floating unit. The components are as described below in eq 1.

$$[M]\{\ddot{x}\} + [B]\{\dot{x}\} + [C]\{x\} = \{F(t)\} \tag{1}$$

Expanded further to accommodate the degree of freedom being investigated within this project scope (i,j=1,2,& 6), however, for the sake of easing the computational procedure, the yaw motion will be represented as i=j=3 instead of 6 during the development of the final equation of motion (eom), this is to avoid a jump during iteration.

$$[m_{ij} + A_{ij}] * \{\ddot{X}_j\} + [B_{ij}] * \{\dot{X}_j\} + [C_{ij} + K_{ij}] * \{X_j\} = \{F_j\} \tag{2}$$

Where;

The virtual mass matrix [M] as shown in equation 3, is composed of the actual mass and added inertial ‘m’ of the unit and the added mass and added inertial ‘A’ components resulting from motions.

$$[M]_{ij} = [m]_{ij} + [A]_{ij} \tag{3}$$

Using the standard form for the structural mass matrix;

$$[m]_{ij} = \begin{bmatrix} m_{11} & m_{12} & m_{16} \\ m_{21} & m_{22} & m_{26} \\ m_{61} & m_{62} & m_{66} \end{bmatrix} \tag{4}$$

Which can be written in actual terms as;

$$[m]_{ij} = \begin{bmatrix} m_{11} & 0 & -y_g * m_{11} \\ 0 & m_{11} & x_g * m_{11} \\ -y_g * m_{11} & -x_g * m_{11} & I_{zz} \end{bmatrix} \tag{5}$$

m_{11} is the structural mass of the unit, the responses (displacement, velocity and acceleration) and force vectors are denoted as:

$$\{X_j\} = \begin{Bmatrix} X_1 \\ X_2 \\ X_6 \end{Bmatrix} \tag{6}, \quad \{\dot{X}_j\} = \begin{Bmatrix} \dot{X}_1 \\ \dot{X}_2 \\ \dot{X}_6 \end{Bmatrix} \tag{7}, \quad \{\ddot{X}_j\} = \begin{Bmatrix} \ddot{X}_1 \\ \ddot{X}_2 \\ \ddot{X}_6 \end{Bmatrix} \tag{8}, \quad \{F_j\} = \begin{Bmatrix} F_1 \\ F_2 \\ F_6 \end{Bmatrix} \tag{9}$$

In the present study, the moment of inertial around the z-axis is estimated as equation 10 using the under-water geometric dimensions of the unit,

$$I_{zz} = I_{66} = \frac{m}{12} * (L_s^2 + B_s^2) \tag{10} \quad \text{or} \quad I_{zz} = m * K_{zz}^2 \tag{11}$$

Using the radius of gyration about the yaw axis.

Estimation of the Excitation Force

The force estimate used for this analysis is limited to the Froude Krylov and the diffraction force on the unit. Approximate equations according [15] adopted. Figure 5 shows the coordinate system used for the development of the force equations.

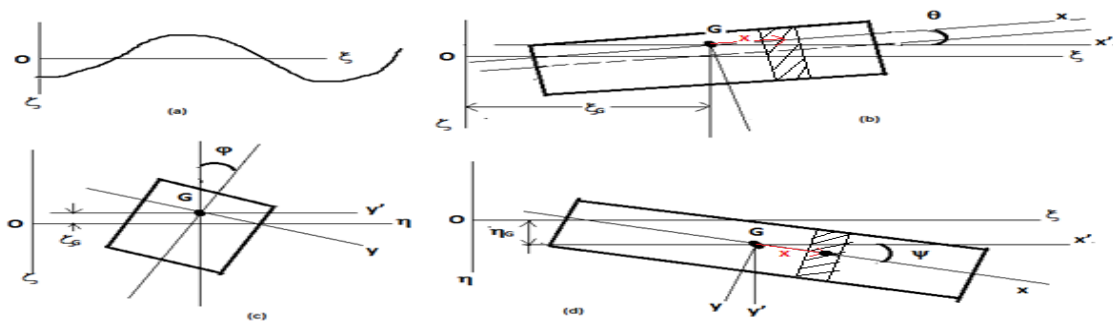


Figure 6 Coordinate system showing a strip at section x from unit centre of gravity

Froude Krylov Force Estimate

The Froude Krylov force assumes that the wave field or pressure is unshattered or undisturbed in the presence of the hull. The approximate equations for the dof under investigation are shown below according to equations 12 to 14

Surge:

$$X_{FK} \cong \rho g \theta \cdot \int_L A(x) \cdot dx - \rho g \cdot \cos(\varphi) \cdot \int_L F(x) \cdot A(x) \cdot \sin(\xi_G + x \cdot \cos(\varphi) - c \cdot t) \cdot dx \tag{12}$$

Sway:

$$Y_{FK} \cong \rho g \cdot \sin(\varphi) \cdot \int_L F(x) \cdot A(x) \cdot \sin(\xi_G + x \cdot \cos(\varphi) - c \cdot t) \cdot dx \tag{13}$$

Yaw:

$$N_{FK} \cong \rho g \cdot \sin(\varphi) \cdot \int_L F(x) \cdot A(x) \cdot x \cdot \sin \{k \cdot (\xi_G + x \cdot \cos(\varphi) - c \cdot t)\} \cdot dx \tag{14}$$

With

$$F(x) = \zeta_\omega \cdot k \cdot \frac{\sin(k \cdot \frac{B(x)}{2} \cdot \sin(\varphi))}{k \cdot \frac{B(x)}{2} \cdot \sin(\varphi)} \cdot e^{-k(\xi_G - x \cdot \theta + \frac{A(x)}{B(x)})} \tag{15}$$

Where:

A(x), B(x) are the wetted area and the breadth of each strip at each instant of time respectively.

c is the wave celerity and k the wave number,

$k = \frac{\omega^2}{g}$ for deep water and $k = \frac{\omega}{\sqrt{gd}}$ is for shallow water (d being the water depth)

ζ_ω is the wave amplitude

ψ is the instantaneous roll angle

θ is the instantaneous pitch angle

φ is the instantaneous yaw angle.

The yaw angle w.r.t the wave direction changes with time in 12-14, and this affects the entire system over every time step.

Diffraction Force Estimate

The diffraction force is the wave force due to the diffracted wave pressure field as a result of the presence of the hull. For a regular wave of frequency ω , the approximate equations for the diffraction forces in sway and yaw are given according to equation 16 and 17.

Sway:

$$Y_{DF} = \int_L \left[m_{22}(x) \frac{d\bar{w}_H}{dt} + b_{22}(x) \bar{w}_H \right] dx \tag{16}$$

Yaw:

$$N_{DF} = \int_L \left[m_{22}(x) \frac{d\bar{w}_H}{dt} + b_{22}(x) \bar{w}_H \right] (x) dx \tag{17}$$

With

$$\bar{w}_H = a.k.c.\sin(\varphi).e^{-k(\xi_G-x.\theta+z'_B(x))}.\cos\{k.(\xi_G+x.\cos(\varphi)-y'_B(x).\sin(\varphi)-c.t)\} \quad (18)$$

$$\bar{w}_V = a.k.c.\sin(\varphi).e^{-k(\xi_G-x.\theta+z'_B(x))}.\sin\{k.(\xi_G+x.\cos(\varphi)-y'_B(x).\sin(\varphi)-c.t)\} \quad (19)$$

$$\bar{w}_R = -a.k^2.c.\sin(\varphi).e^{-k(\xi_G-x.\theta+z'_B(x))}.\cos\{k.(\xi_G+x.\cos(\varphi)-y'_B(x).\sin(\varphi)-c.t)\} \quad (20)$$

Differentiating to get the corresponding accelerations;

$$\frac{d\bar{w}_H}{dt} = a.k^2.c^2.\sin(\varphi).e^{-k(\xi_G-x.\theta+z'_B(x))}.\sin\{k.(\xi_G+x.\cos(\varphi)-y'_B(x).\sin(\varphi)-c.t)\} \quad (21)$$

$$\frac{d\bar{w}_V}{dt} = -a.k^2.c^2.\sin(\varphi).e^{-k(\xi_G-x.\theta+z'_B(x))}.\cos\{k.(\xi_G+x.\cos(\varphi)-y'_B(x).\sin(\varphi)-c.t)\} \quad (22)$$

$$\frac{d\bar{w}_R}{dt} = -a.k^3.c^2.\sin(\varphi).e^{-k(\xi_G-x.\theta+z'_B(x))}.\sin\{k.(\xi_G+x.\cos(\varphi)-y'_B(x).\sin(\varphi)-c.t)\} \quad (23)$$

y'_B and z'_B are the coordinate of the centroid of the instantaneous wetted hull strip.

The equations 16 and 17 can be easily solved for the appropriate values of the respective diffraction forces at every time step, hence a time varying diffraction force is obtained which is then added to the Froude Krylov force to get the total force before solving the motion equation.

Estimating the added mass, damping and stiffness matrix coefficients

The virtual mass matrix and the damping coefficients are the hydrodynamic coefficients significant in the determination of the dynamic behavior of the unit in wave. The virtual mass is composed of the actual mass and inertial 'm or I' of the unit and the added mass and added inertial 'A' components resulting from motions.

For moored FPSO with large number of initially taut or tensioned tethers, the values of the mass of the unit changes slightly by taking up the adherent mass of the slacked polyester lines. This mass however is negligible compared to the structural mass of the unit and thus cannot be added to the unit mass for the purpose of computation. In the present studies, restoring capability is enabled by the taut lines depending on the number been used. Thus, the restoring coefficient is estimated based on the number of lines and configuration used.

Determination of the Added Mass and Inertia Matrix

The standard simplified Lewis Conformal Mapping was used to estimate the added mass terms. The 2D Strip theory is used in this form, to estimate the 2D added mass and inertial coefficients which are then integrated over the length to determine the 3D Coefficients. The procedure according to [16] was implemented to compute the scale factor μ_s , and Lewis' coefficients a_1 and a_3 . These values are then used as input values in the computation of 2D added mass for some of the motion states. See equations below;

Sway

$$\mu_{22} = \frac{\pi\rho}{2}\mu_s^2 [(1-a_1)^2 + 3a_3^2] \quad (24)$$

Sway –Roll

$$\mu_{24} = 4\rho\mu_s^3 \left[\frac{1}{3}a_1(1-a_1)(1+a_1) + a_3 \left[\frac{3}{5}(1+a_3) + \frac{4}{15}a_3(1-a_1) - \frac{6}{7}a_3 \right] \right] \quad (25)$$

Heave;

$$\mu_{33} = \frac{\pi\rho}{2}\mu_s^2 [(1+a_1)^2 + 3a_3^2] \quad (26)$$

Roll;

$$\mu_{44} = \pi\rho\mu_s^4 [a_1^2(1+a_1)^2 + 2a_3^2] \quad (27)$$

The non-zero added mass/inertial is then approximated using twenty-one (21) mid-ship sections equally spaced at Δx . Note that for a stationary unit, like the FPSO its velocity $u=0$. This reduces the equation as presented by [16] to those of equation 28 below.

$$\left. \begin{aligned}
 A_{33} &= \sum \mu_{33} \Delta x \\
 A_{35} &= \sum x \cdot \mu_{33} \cdot \Delta x \\
 A_{53} &= \sum x \cdot \mu_{33} \cdot \Delta x \\
 A_{55} &= \sum x^2 \cdot \mu_{33} \cdot \Delta x \\
 A_{22} &= \sum \mu_{22} \cdot \Delta x \\
 A_{24} &= A_{42} = \sum \mu_{24} \Delta x \\
 A_{26} &= A_{62} = \sum x \cdot \mu_{22} \cdot \Delta x \\
 A_{44} &= \sum \mu_{44} \cdot \Delta x \\
 A_{46} &= A_{64} = \sum x \cdot \mu_{24} \cdot \Delta x \\
 A_{66} &= \sum x^2 \cdot \mu_{22} \cdot \Delta x
 \end{aligned} \right\} \tag{28}$$

Combining the elements of equation 24 and 27 the virtual mass matrix of equation 28 can be estimated at the given time step.

Other approximate techniques can be applied to determine the diagonal elements of the added mass matrix. See [17] for elaborate procedure.

The final added mass matrix is then represented as;

$$[A]_{ij} = \begin{bmatrix} A_{11} & A_{12} & A_{16} \\ A_{21} & A_{22} & A_{26} \\ A_{61} & A_{62} & A_{66} \end{bmatrix} = \begin{bmatrix} 0 & 0 & 0 \\ 0 & A_{22} & A_{26} \\ 0 & A_{62} & A_{66} \end{bmatrix} \tag{29}$$

The cross-sectional areas were obtained from the generalized form of the trapezium rule for unequal intervals applied to the offset points for each section. This brings the virtual mass matrix to

$$[M]_{ij} = \begin{bmatrix} m_{11} & 0 & -y_g * m_{11} \\ 0 & m_{11} + A_{22} & x_g * m_{11} + A_{26} \\ -y_g * m_{11} & -x_g * m_{11} + A_{62} & I_{zz} + A_{66} \end{bmatrix} \tag{30}$$

Damping coefficient approximation

Sway;

$$b_{22} = \rho \cdot \omega \cdot I_{22} \cdot D_s^2 \tag{31}$$

Heave;

$$b_{33} = \rho \cdot \omega \cdot I_{33} \cdot B_s^3 \tag{32}$$

Roll;

$$b_{44} = \rho \cdot \omega \cdot I_{44} \cdot D_s^4 \tag{33}$$

Sway-Roll;

$$b_{24} = \rho \cdot \omega \cdot I_{24} \cdot D_s^3 \tag{34}$$

Were I_{ij} , D_s , B_s are the non-dimensional mass/Inertial coefficient of the ship form, the Lewis form draft and beam respectively.

For a regular wave of frequency ω , the time variant parameters in the equation include $D_s(t)$, $B_s(t)$, $I_{ii}(t)$. These values are thus used within the time loop and are recomputed at every time step.

For the regular wave scenario, the equations 25 to 34 can be easily solved for the appropriate values of the respective 2D damping coefficients at every time step, hence time varying value is obtained. The non-zero 3D damping coefficient can then be approximated using a predetermined odd number of mid-ship sections (21 strips) equally spaced at Δx . These values are then used to form the damping matrix before solving the resulting motion equation. Note that for a stationary unit, like the FPSO, $U \approx 0$. This again modifies the equation according to [16] to those of equation 35.

$$\left. \begin{aligned}
 B_{33} &= \sum b_{33} \Delta x \\
 B_{35} &= \sum x \cdot b_{33} \cdot \Delta x \\
 B_{53} &= \sum x \cdot b_{33} \cdot \Delta x \\
 B_{55} &= \sum x^2 \cdot b_{33} \cdot \Delta x \\
 B_{22} &= \sum b_{22} \cdot \Delta x \\
 B_{24} &= B_{42} = \sum b_{24} \Delta x \\
 B_{26} &= B_{62} = \sum x \cdot b_{22} \cdot \Delta x \\
 B_{44} &= \sum b_{44} \cdot \Delta x \\
 B_{46} &= B_{64} = \sum x \cdot b_{24} \cdot \Delta x \\
 B_{66} &= \sum x^2 \cdot b_{22} \cdot \Delta x
 \end{aligned} \right\} \tag{35}$$

Combining the elements of equation 31 - 34 and 35, the non-zero 3D potential damping coefficient matrix of the eom can be solved at any given time step. Thus, the final damping matrix (potential damping) excluding the structural damping reduces to

$$[B]_{ij} = \begin{bmatrix} B_{11} & B_{12} & B_{16} \\ B_{21} & B_{22} & B_{26} \\ B_{61} & B_{62} & B_{66} \end{bmatrix} = \begin{bmatrix} 0 & 0 & 0 \\ 0 & B_{22} & B_{26} \\ 0 & B_{62} & B_{66} \end{bmatrix} \quad (36)$$

Restoring coefficient

Restoring coefficient matrix resulting from the free floating FPSO (CC_{ij}) is modified by the restoring force introduced from the mooring lines stiffness K_{ij} to give the final restoring coefficient matrix (C_{ij}). It is significant to note that, without any form of fixation of unit, there is hardly any restoring against the surge, sway and yaw motion modes from the unit-wave interaction. The equation of the restraining matrix is given by equation 35,

$$C_{ij} = CC_{ij} + K_{ij} \quad (37)$$

Using standard equations with parameters given, the non-zero elements of the CC_{ij} matrix can easily be approximated thus;

$$\left. \begin{aligned} CC_{33} &= \rho g S_0 \quad \text{or} \quad \rho g \int B_S(x) dx \\ CC_{35} &= \rho g x_f S_0 \quad \text{or} \quad -\rho g \int x \cdot B_S(x) dx \\ CC_{55} &= \rho g I_y \quad \text{or} \quad \rho g \int x^2 \cdot B_S(x) dx \\ CC_{44} &= \rho g \cdot \nabla \cdot \overline{GM_T} \end{aligned} \right\} \quad (38)$$

Thus, the final restoring from the free-floating unit w.r.t the motions under consideration is thus;

$$[CC]_{ij} = \begin{bmatrix} CC_{11} & CC_{12} & CC_{16} \\ CC_{21} & CC_{22} & CC_{26} \\ CC_{61} & CC_{62} & CC_{66} \end{bmatrix} = \begin{bmatrix} 0 & 0 & 0 \\ 0 & 0 & 0 \\ 0 & 0 & 0 \end{bmatrix} \quad (39)$$

Approximating the Restoring Coefficient contribution from mooring Taut Tethers

The unit is assumed to be moored using a taut tether instead of a steel catenary system. Taut polyester mooring lines are light, and produce their restoring force via a pre-tension technique which is applied to it. It has more advantages in terms of economy and safety of operations. The method adopted is found in [18]. The capacity to restore is due to the elastic nature of the material with elastic stiffness λ .

The overall stiffness from the entire mooring lines is represented by

$$K_{ij} = \sum_{q=1}^{q=Nm} k_{ij}^q \quad (40)$$

Where;

k_{ij}^q is the stiffness matrix for a single mooring line.

Nm is the number of mooring lines used.

For a single mooring line, with a pre-determined pre-tension T.

$$T = \frac{MBL}{SF} \quad (41)$$

MBL – maximum breaking load of polyester material

SF – recommended safety factor

Two attachment points (the fairlead and anchor points) are established or approximated using the depth of water D and the attachment angle at the sea bed.

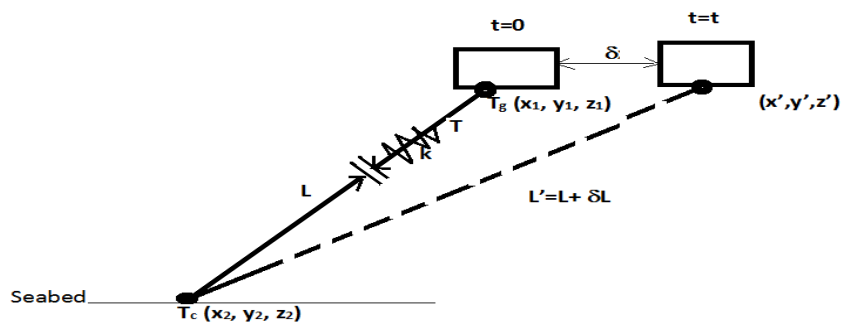


Figure 7 Mooring line motion resulting from moving FPSO

At the initial position i.e., time (t)=0, when all lines are taut, the restoring force is defined by the direction cosines. For a single line index ‘q’

With

$$\left. \begin{aligned} a_T &= x_2 - x_1 \\ b_T &= y_2 - y_1 \\ c_T &= z_2 - z_1 \end{aligned} \right\} \quad (42)$$

$$\left. \begin{aligned} l_x &= \cos(\alpha) = \frac{a_T}{L} \\ l_y &= \cos(\beta) = \frac{b_T}{L} \\ l_z &= \cos(\gamma) = \frac{c_T}{L} \end{aligned} \right\} \quad (43)$$

Initial length of taut tether is;

$$L = \sqrt{a_T^2 + b_T^2 + c_T^2} \quad (44)$$

Due to the small motion δx , new tether length to 1st order approximation gives;

$$L' = L + \delta L = L + \frac{a_T}{L} \cdot \delta x \quad (45)$$

This will create additional tension, that can be evaluated as shown below;

$$\delta T = \lambda \cdot \delta L = \lambda \cdot \frac{a_T}{L} \cdot \delta x \quad (46)$$

Thus, the resulting restoring force component in x-direction can be represented as;

$$\delta T_x = (T + \delta T) \cos(\alpha') - T \cos(\alpha) \quad (47)$$

Where the direction cosine in new position (2) is then obtained

$$\cos(\alpha') = \frac{a_T + \delta x}{L'} \quad (48)$$

$$\therefore T_x = (T + \delta T) \frac{a_T}{L'} \left[\frac{1 + \delta x/a_T}{1 + \delta L/L} \right] - T \frac{a_T}{L} \quad (49)$$

$$T_x = T \cos(\alpha) \cdot \left\{ \frac{\delta x}{a_T} - \frac{\delta L}{L} + \frac{\delta T}{T} \right\} \quad (50)$$

Approximating to first order, with the change in length given as;

$$\delta L \approx \delta x \cdot l_x \quad (51)$$

$$\delta T_x = \frac{T}{L} l_x \left[\frac{L \cdot \delta x}{a_T} - l_x \cdot \delta x + \frac{\lambda \cdot a_T}{T} \cdot \delta x \right] \quad (52)$$

$$\delta T_x = \lambda \cdot l_x^2 + \frac{T \cdot \sin^2(\alpha) \cdot \delta x}{L} = \lambda \cdot l_x^2 + \frac{T \cdot (1 - l_x^2) \cdot \delta x}{L} \quad (53)$$

The first stiffness term is defined as the limit expression of equation 55

$$k_{11}^q = \lim_{\delta x \rightarrow 0} \left[\frac{\partial T_x}{\partial x} \right] \quad (54)$$

This is then approximated as;

$$k_{11}^q = \lambda \cdot l_x^2 + \frac{T}{L} \quad (55)$$

Other terms are estimated accordingly following similar procedure, thus;

$$\left. \begin{aligned} k_{21}^q &= \left[\lambda + \frac{T}{L} \right] \cdot l_x \cdot l_y \\ k_{12}^q &= k_{21}^q \\ k_{31}^q &= \left[\lambda + \frac{T}{L} \right] \cdot l_x \cdot l_z \\ k_{13}^q &= k_{31}^q \\ k_{22}^q &= \lambda \cdot l_y^2 + \frac{T}{L} [1 - l_y^2] \\ k_{32}^q &= \left[\lambda + \frac{T}{L} \right] \cdot l_y \cdot l_z \\ k_{23}^q &= k_{32}^q \\ k_{33}^q &= \lambda \cdot l_z^2 + \frac{T}{L} [1 - l_z^2] \end{aligned} \right\} \quad (56)$$

The remaining terms in the 6 X 6 matrix are computed as functions of the ones already estimated above;

$$\left. \begin{aligned}
 k_{41}^q &= k_{14}^q = k_{31}^q * y_2 - k_{21}^q * z_2 \\
 k_{51}^q &= k_{15}^q = k_{11}^q * z_2 - k_{31}^q * x_2 \\
 k_{61}^q &= k_{16}^q = k_{21}^q * x_2 - k_{11}^q * y_2 \\
 k_{52}^q &= k_{25}^q = k_{21}^q * z_2 - k_{32}^q * x_2 \\
 k_{62}^q &= k_{26}^q = k_{22}^q * x_2 - k_{21}^q * y_2 \\
 k_{43}^q &= k_{34}^q = k_{33}^q * y_2 - k_{32}^q * z_2 \\
 k_{53}^q &= k_{35}^q = k_{31}^q * z_2 - k_{33}^q * x_2 \\
 k_{63}^q &= k_{36}^q = k_{32}^q * x_2 - k_{31}^q * y_2 \\
 k_{44}^q &= k_{33}^q * y_2^2 - 2k_{32}^q * y_2 * z_2 + k_{22}^q * z_2^2 \\
 k_{54}^q &= k_{45}^q = k_{31}^q * y_2 * z_2 - k_{21}^q * z_2^2 + k_{33}^q * y_2 * x_2 + k_{32}^q * x_2 * z_2 \\
 k_{64}^q &= k_{46}^q = k_{32}^q * y_2 * x_2 - k_{22}^q * z_2 * x_2 - k_{31}^q * y_2^2 + k_{21}^q * y_2 * z_2 \\
 k_{55}^q &= k_{11}^q * z_2^2 - 2k_{31}^q * x_2 * z_2 + k_{33}^q * x_2^2 \\
 k_{65}^q &= k_{56}^q = k_{21}^q * z_2 * x_2 - k_{32}^q * x_2^2 - k_{11}^q * y_2 * z_2 + k_{31}^q * y_2 * x_2 \\
 k_{66}^q &= k_{22}^q * x_2^2 - 2k_{21}^q * y_2 * x_2 + k_{11}^q * y_2^2
 \end{aligned} \right\} \tag{57}$$

The above procedure is repeated for all other lines (q=1: Nm). It is important to note that the fairlead position is radially spaced around the turret base radius for all the lines, the anchor point at the sea bed varies for each line as well. The mooring line restoring matrix K_{ij} is estimated thus using equation 39 for 3-dof been considered as thus;

$$[K]_{ij} = \begin{bmatrix} K_{11} & K_{12} & K_{16} \\ K_{21} & K_{22} & K_{26} \\ K_{61} & K_{62} & K_{66} \end{bmatrix} = \begin{bmatrix} \sum_{q=1}^{q=Nm} k_{11}^q & \sum_{q=1}^{q=Nm} k_{12}^q & \sum_{q=1}^{q=Nm} k_{16}^q \\ \sum_{q=1}^{q=Nm} k_{21}^q & \sum_{q=1}^{q=Nm} k_{22}^q & \sum_{q=1}^{q=Nm} k_{26}^q \\ \sum_{q=1}^{q=Nm} k_{61}^q & \sum_{q=1}^{q=Nm} k_{62}^q & \sum_{q=1}^{q=Nm} k_{66}^q \end{bmatrix} \tag{58}$$

To calculate the total stiffness, equation 59 is used

$$C_{ij} = CC_{ij} + K_{ij} = \begin{bmatrix} \sum_{q=1}^{q=Nm} k_{11}^q & \sum_{q=1}^{q=Nm} k_{12}^q & \sum_{q=1}^{q=Nm} k_{16}^q \\ \sum_{q=1}^{q=Nm} k_{21}^q & \sum_{q=1}^{q=Nm} k_{22}^q & \sum_{q=1}^{q=Nm} k_{26}^q \\ \sum_{q=1}^{q=Nm} k_{61}^q & \sum_{q=1}^{q=Nm} k_{62}^q & \sum_{q=1}^{q=Nm} k_{66}^q \end{bmatrix} \tag{59}$$

Since for this study, $CC_{ij} = [0]$

Numerical computation to the Equation of Motion

The final equation of motion to be solved is a 3 dof 2nd order differential equation. It is of the form in equation 2, $[m_{ij} + A_{ij}] * \{\ddot{X}_j\} + [B_{ij}] * \{\dot{X}_j\} + [C_{ij} + K_{ij}] * \{X_j\} = \{F_j\}$

Substituting equations, 6 to 9, 29, 35 and 59 yields the eom as shown in equation 60.

$$\begin{bmatrix} m_{11} & 0 & -y_g * m_{11} \\ 0 & m_{11} + A_{22} & x_g * m_{11} + A_{26} \\ -y_g * m_{11} & -x_g * m_{11} + A_{62} & I_{zz} + A_{66} \end{bmatrix} \begin{Bmatrix} \ddot{X}_1 \\ \ddot{X}_2 \\ \ddot{X}_6 \end{Bmatrix} + \begin{bmatrix} 0 & 0 & 0 \\ 0 & B_{22} & B_{26} \\ 0 & B_{62} & B_{66} \end{bmatrix} \begin{Bmatrix} \dot{X}_1 \\ \dot{X}_2 \\ \dot{X}_6 \end{Bmatrix} + \begin{bmatrix} \sum_{q=1}^{q=Nm} k_{11}^q & \sum_{q=1}^{q=Nm} k_{12}^q & \sum_{q=1}^{q=Nm} k_{16}^q \\ \sum_{q=1}^{q=Nm} k_{21}^q & \sum_{q=1}^{q=Nm} k_{22}^q & \sum_{q=1}^{q=Nm} k_{26}^q \\ \sum_{q=1}^{q=Nm} k_{61}^q & \sum_{q=1}^{q=Nm} k_{62}^q & \sum_{q=1}^{q=Nm} k_{66}^q \end{bmatrix} \begin{Bmatrix} X_1 \\ X_2 \\ X_6 \end{Bmatrix} = \begin{Bmatrix} F_1 \\ F_2 \\ F_6 \end{Bmatrix} \tag{60}$$

The mathematical model representing the system is solved using the Runge-Kutta Carskarp multistep method after the application of the state space method.

The methods solution algorithm is designed for fixed time step. For the Runge-Kutta methods, the 3dof 2nd ODE was first converted into two 1st ODEs using the state space technique, after which they are numerically solved.

Motion Time history Analysis Technique

The output from the motion simulator is the time histories of the displacements, velocities and accelerations (translational and rotational), forces or moments. Time series data are treated differently from the other conventional data sets.

The wave input as well as the generated response are produced as time series from the various simulation channels. The raw data can be directly visualized from the time history or Fourier analysis carried out on them to enable conversion into the frequency domain for visualization. The direct first-hand visualization of the time series is significant for use in assessing the global validity of the simulation or test, in which the amplitude and critical periods are estimated. In a similar manner, the visualized frequency domain data is used

to decide the possibility of using a filter with the knowledge of the response frequencies and perhaps the noise level also [19].

Some of the descriptive statistics obtainable directly from the time series or the spectra density curve used for the evaluation of the response include the average (a_0), maximum (x_{max}) and minimum (x_{min}), i.e., range ($x_{max} - x_{min}$), the variance (m_0) or standard deviation (σ). In addition to these statistics, the spectra moments (m_n) is also required from the spectra density curve. The significant value ($y_{1/3}$), average period (T_1), and average zero crossing period (T_2) of response are estimated thus.

$$m_n = \int_0^\infty \omega^n S(\omega) \cdot d\omega \tag{62}$$

$$(n=0,1,2,4)$$

$$\left. \begin{aligned} \sigma &= \sqrt{m_0} \\ y_{1/3} &= 4\sigma \\ T_2 &= \sqrt{\frac{m_0}{m_2}} \\ T_1 &= \frac{m_0}{m_1} \end{aligned} \right\} \tag{63}$$

For the irregular wave and associated irregular time series, the spectra density can be obtained by using the power density function (PSD), according to [20] and [21]

Dimensions and Data of FPSO, Wave and Mooring lines

Principal dimensions of the FPSO

- Length 206.75m
- Beam 38.4m
- Hull depth 30.08m
- Hull form coefficients ($C_b=0.843, C_p =0.80, C_{am}=0.90$)

Mooring Line Data		Wave Characteristics	
D_r	245mm	Elevations	6m, 4m and 2m
MBL	20307KN	Frequency	0.3, 0.4, 0.5, 0.6 (rad/s)
EA	599000KN	Period	20.93, 15.7, 12.56, 10.46 (s)
SF	1.82	Shallow water depth	300m
ML_a	40.7kg/m	Deep water depth	1028m
ML_{h2o}	9.4kg/m		
S_g	1.38		
Stiffness	310.6707KN/m (SINGLE LINE)		

The above data were used in the MATLAB routine, to solve for the various output parameters and the displacement response extracted for statistical evaluation and these results were further validated using ORCAFLEX

IV. RESULT AND DISCUSSION

Variation of response in shallow and deep water

The figures below are derived statistically from the time series of the different runs using the MATLAB code;

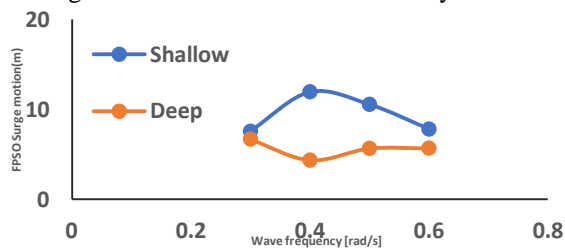


Figure 8 Surge motion comparison for deep and shallow water at $z = 6m$

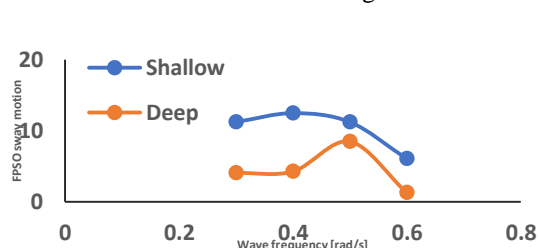


Figure 9 Sway motion comparison for deep and shallow water at $z = 6m$

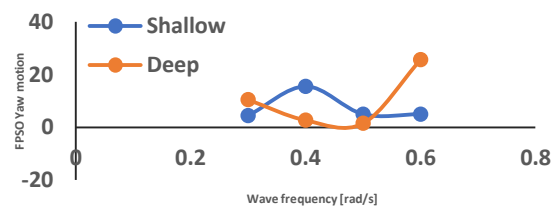


Figure 10 Yaw motion comparison for deep and shallow water at $z = 6m$

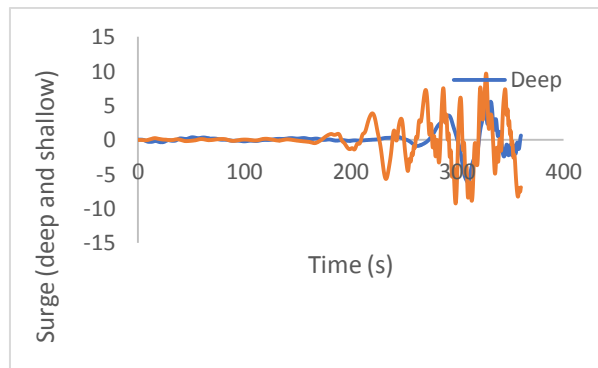


Figure 11 Surge response in deep and shallow water [6m, 0.5rad/s]

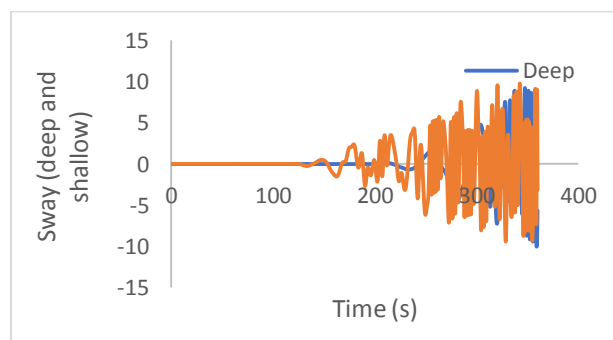


Figure 12 Sway response in deep and shallow water [6m, 0.5rad/s]

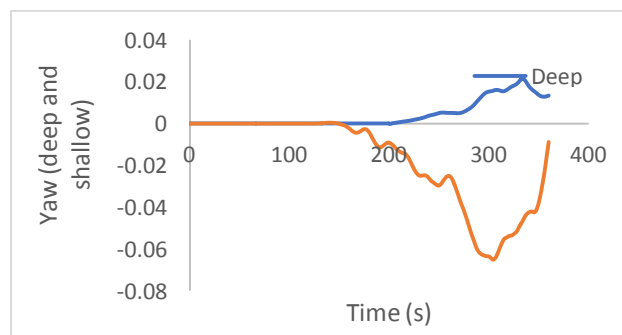


Figure 13 Yaw response in deep and shallow water [6m, 0.5rad/s]

To validate the analysis carried out using MATLAB, a further analysis was carried out using ORCAFLEX for a frequency of 0.6 rad/s, period of 20.94s and a water depth of 1200m. The results are shown below and further explained afterwards.

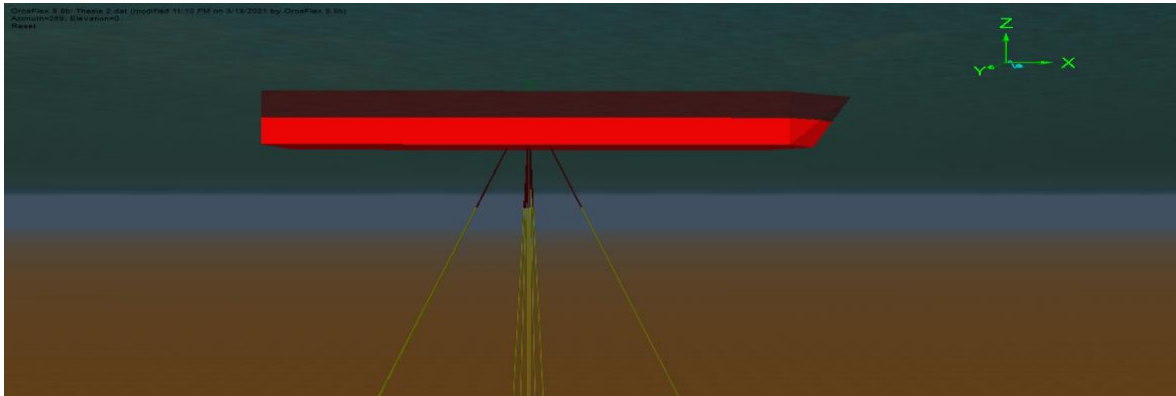


Figure 14 3D ORCAFLEX Model

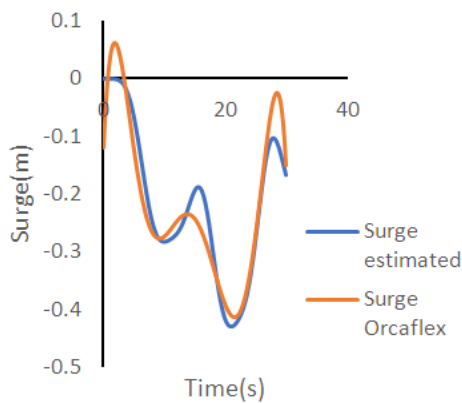


Figure 15 Surge response – MATLAB/ORCAFLEX

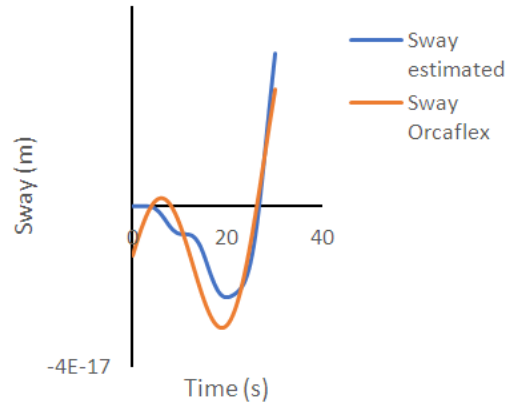


Figure 16 Sway response –

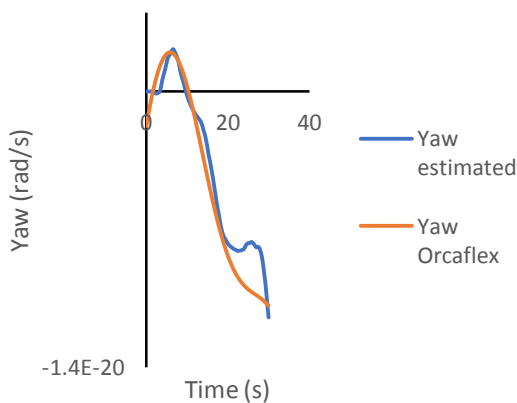


Figure 17 Yaw response – MATLAB/ORCAFLEX

Motion mode		MATLAB estimate	ORCAFLEX	%error
surge	std	0.128050279	0.133520339	
	sig. value	0.512201114	0.534081354	-4.10
sway	std	1.2692E-17	1.44481E-17	
	sig. value	5.07678E-17	5.77924E-17	-12.15
yaw	std	4.00203E-21	4.73975E-21	
	sig. value	1.60081E-20	1.8959E-20	-15.56

Table 1 Error Calculation between both methods

The goodness of fit between the two methods as captured by the validation plots of figures 14 to 16 showed that the regression between MATLAB and ORCAFLEX is between 0.91, 0.85 and 0.95 for the surge, sway and yaw motions respectively.

III. CONCLUSION

FPSO's have become a leading engineering system for offshore operations in shallow, deep and even ultra-deep waters ranging from water depths of 50m to above 3000m and its versatility cannot be overlooked, however there are so many different factors that can affect the motion response of the FPSO and as it continues to remain an important aspect of the engineering system there needs to be continuous studies on the reasons for

the different challenges that the FPSO undergoes and solutions to combat such challenges or minimize the effect of the challenge.

As can be recalled, RAO's which stands for response amplitude operator is a statistical phenomenon used in the marine/offshore industry to measure the behavior of the FPSO operating at sea. This was derived using a time series evaluation and while a Fourier series technique could be used to interpret the time series evaluation a statistical approach was used.

From the results above it can be seen that within the envelope of the analysis (frequency range: 0.3 rad/s – 0.6 rad/s and wave elevation: 2m – 6m) the same vessel responds differently in shallow and deep water, however this project was dedicated to motion response in 3 degrees of freedom (Surge, Sway and Yaw), and from the analysis it can be seen that the surge, sway and yaw forces are responsible for the vessel response in the surge, sway and yaw directions furthermore, it can be observed that majority of the time the surge, sway and yaw motion responses in shallow water seem to be greater than that of deep water and this is often the result of the water depth as the velocity of the water in shallow water has greater effect than in deep water due to the water depth, also the deep water conditions allows for better damping from the mooring lines which reduces the force on the vessel and its corresponding motion effect.

Knowing this, that the motion response in shallow water is more than that of deep water, engineers need to take care in the design and operation of an FPSO in shallow water scenario such that during the life span of the FPSO at field (25 years) the vessel should be able to withstand the pressure forces acting on it without undergoing failure.

REFERENCES

- [1]. (2011). E&P Magazine.
- [2]. (2013). Saipem Magazine
- [3]. (2013). Offshore Magazine.
- [4]. Chakrabarti, S. (2005). Handbook of offshore Engineering , volume II, Plainfield, Illinois, USA.
- [5]. Young Luo, S. B. (2003). Predicting FPSO Responses Using Model Tests and Numerical Analysis.
- [6]. Xin Li, J. Y. (2003). Motion Analysis on a Large FPSO in Shallow Water.
- [7]. Montsair Osman Ahmed Ali, I. A. (2019). Effects of water depth, mooring line diameter and hydrodynamic coefficients on the behaviour of deepwater FPSO's.
- [8]. Marc Vantorre, K. (2017). Manuevering in Shallow and Confined water. Encyclopedia of Maritime and Offshore Engineering.
- [9]. Ghent University(n.d).
- [10]. McTaggart, K. (2016). Literature Review for Design and Assessment of Directional Stability and Turning Performance of Naval Defenders. Defence Research and Development Canada
- [11]. Matthew Guan, M. O. (2018). Effect of Water Depths on the Hydrodynamic Responses of an FPSO Platform, MATEC Web Conferences. EDP Sciences
- [12]. Keprate, A. (2014). Appraisal of Riser Concepts for FPSO in Deepwater.
- [13]. Arun S. Duggai, Y. A. (2004). Global Analysis of Shallow Water FPSO's.
- [14]. Osalusi, E. (2020). Shallow Water Offshore: Sea Eagle FPSO Metocean Reference Document.
- [15]. Ming-Chung Fang, J.-H. L.-L. (2005). A Nonlinear Mathematical Model for Ship Turning Circle Simulation in Waves.
- [16]. Ciobanu Camelia and Anghel Arlene-Rabela,(2008), "The computing of the damping generalized coefficient", Proceedings of the Romania Academy, Series A, vol.9, No.3.
- [17]. Bishops R.E.D., and Prize W.G.,(1979), ' Hydroelasticity of Ships', Cambridge University Press, pg.126.
- [18]. Nina Morgan (1990), 'Marine Technology Reference book', Butterworths, London.
- [19]. Orji. C. U (2019). Motion Response Analysis of FPSO in Multidirectional Seas: The west African offshore region.
- [20]. Newland D.E.,(1993), 'An introduction to random vibrations and spectra analysis', 3rd edition, Published by Longman, London.
- [21]. Roberts J.B and Spanos P.D., (1990), ' Random vibration and statistical linearization', Published by John Wisley & Son's Ltd, England.

Dokubo, Daniel Koriota-a, et. al. "Operational Station Horizontal Plane Motion Maneuvering of FPSO in Shallow and Deep Water." *American Journal of Engineering Research (AJER)*, vol. 10(6), 2021, pp. 108-122.